

Orbitally-driven insulator-metal transition in CuIr_2S_4 : Temperature dependent transient reflectivity study

M. Naseska,¹ P. Sutar,¹ D. Vengust,¹ S. Tsuchiya,^{1,2} M. Čeh,³ D. Mihailovic,^{1,4} and T. Mertelj^{1,4,*}

¹Complex Matter Department, Jozef Stefan Institute, Jamova 39, 1000 Ljubljana, Slovenia

²Department of Applied Physics, Hokkaido University, Sapporo, Japan

³Centre for Electron Microscopy, Jozef Stefan Institute, Jamova 39, 1000 Ljubljana, Slovenia

⁴Center of Excellence on Nanoscience and Nanotechnology Nanocenter (CENN Nanocenter), Jamova 39, 1000 Ljubljana, Slovenia

(Dated: February 24, 2020)

Ultrafast transient reflectivity across the unusual three-dimensional Peierls-like insulator-metal (IM) transition in CuIr_2S_4 was measured as a function of temperature. The low-temperature insulating-phase transient response is dominated by broken-symmetry-induced coherent lattice oscillations that abruptly vanish at the IM transition. The coherent mode spectra are consistent with Raman spectra reported in literature. The origin of the broken-symmetry-induced is also briefly discussed.

I. INTRODUCTION

The spinel-structure compounds CuIr_2S_4 and MgTi_2O_4 ^{1,2} show unusual, presumably orbitally-driven,³ three-dimensional Peierls-like metal-insulator transitions on cooling at $T_{\text{IM}} \sim 230$ K and ~ 260 K, respectively. The transitions are accompanied with a long range charge ordering forming Ir (Ti) dimers^{4,5} and a strong decrease of the magnetic susceptibility^{2,6}.

The lattice dynamical aspects of the the phase transition in CuIr_2S_4 were studied by means of the Raman spectroscopy⁷⁻⁹ and transient reflectivity⁹. It has been suggested⁸ that the phonons associated with the S-S bonds play a role in the unusual IM phase transition so a more detailed insight into the lattice dynamical properties could be beneficial for understanding the mechanism underlying the transition.

In Raman spectra several additional low frequency modes⁷ appear in the low- T insulating state in addition to the four characteristic spinel-structure modes observed in the high- T cubic metallic state. The frequencies of these modes are, however, not consistent with the coherent transient-reflectivity modes observed in an earlier transient reflectivity study⁹ in neither of the phases.

The difference might be related to the low temperature X-ray- and visible-light-induced conducting phase¹⁰⁻¹⁴ with persistent dimerization^{10,15} and suppressed long range order due to different optical excitation in Raman and transient reflectivity experiments. To resolve the discrepancy and get better insight into the low frequency lattice dynamics across the insulator-metal (IM) transition in CuIr_2S_4 we performed a detailed temperature dependent transient reflectivity study combined with room- T Raman spectroscopy characterization.

We find that the transient reflectivity at 1.55-eV photon energy in the low- T insulating (I) phase is dominated by the coherent lattice response that abruptly vanishes at the IM transition. The frequencies of the observed coherent modes are different than in the previous transient reflectivity study⁹ and are consistent with the frequencies

of the modes observed⁷ by the Raman spectroscopy.

II. EXPERIMENTAL

A. Methods and sample characterization

Single crystals of CuIr_2S_4 were grown from Bi solution as described in Ref. [16]. The crystal structure of the obtained millimeter-size crystals was checked by means of X-ray diffraction. The quality of the crystals was evaluated also by means of Raman scattering using 488-nm

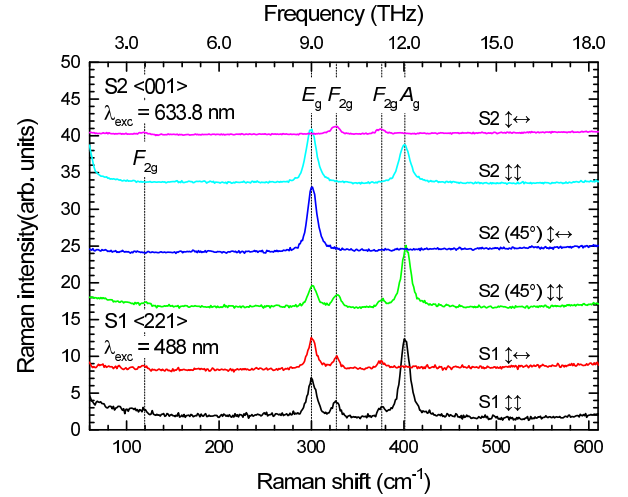


Figure 1. Room- T micro-Raman spectra from cleaved crystal surfaces taken in the back-scattering geometry. For sample S1 the in-plane excitation-light polarization was random while for sample S2 the polarization was either along [100] or [110]. The only A_g mode⁷ at 403 cm^{-1} is always absent in the crossed polarization spectra at both surface orientations while the the E_g mode at 302 cm^{-1} and the two F_{2g} modes at 327 and 375 cm^{-1} are extinct only for polarizations along certain high symmetry directions on the sample-S2 [001] surface. The traces are vertically offset for clarity.

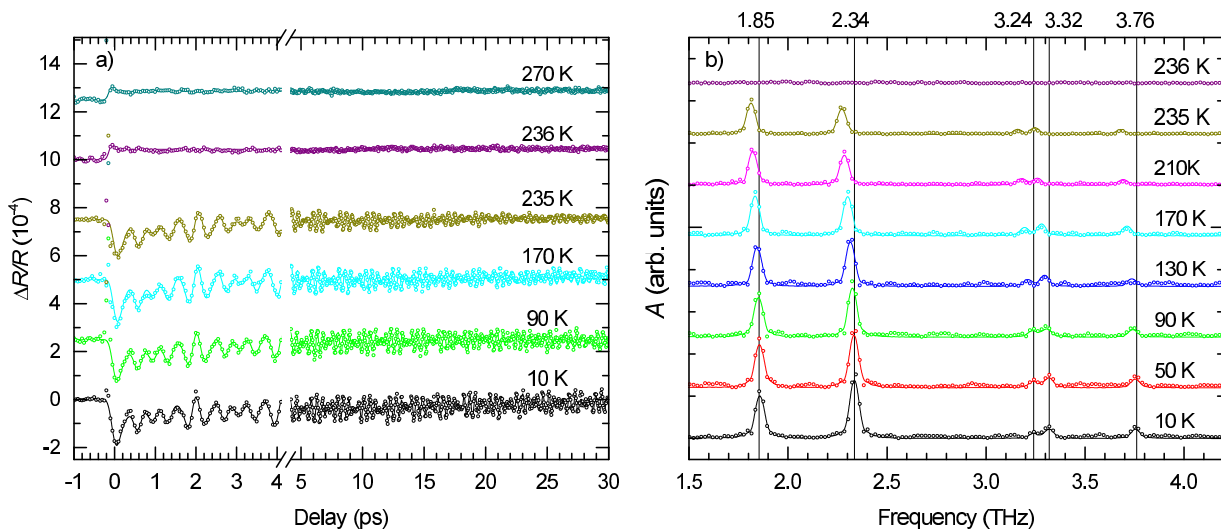


Figure 2. a) The low-excitation-fluence transient reflectivity at selected temperatures during the warming cycle in sample S1. Some coherent artifacts due to the pump scattering are observed around zero delay. b) Fourier transforms of the transient reflectivity at selected temperatures during the warming cycle. The thin lines correspond to the DECP fits discussed in text. Traces at different T are vertically offset for clarity.

and 632.8-nm laser excitation. Room- T Raman spectra from as-grown crystal facets showed four phonon lines at frequencies consistent with previous results⁷, but somewhat broader. Polishing resulted in even broader Raman lines. Cleaved surfaces, on the other hand, showed significantly narrower and more intense Raman phonon lines (see Fig. 1) with an additional weak line at 120 cm^{-1} and were used for all further optical measurements.

Here we present data from two cleaved crystals designated S1 and S2. The orientation of the S1 cleaved surface was determined *a posteriori* from EBSD Kikuchi patterns to be close to the $\langle 221 \rangle$ plane while the orientation of the S2 cleaved surface was inferred from the Raman selection rules to be close to the $\langle 001 \rangle$ plane.

The transient reflectivity measurements were performed using a standard pump-probe setup using 50-fs linearly polarized laser pulses at 800 nm wavelength and the 250 kHz repetition rate as presented in detail elsewhere.¹⁷ Both the pump- and probe-photon energy were at the laser fundamental, $\hbar\omega = 1.55 \text{ eV}$. The transient reflectivity, $\Delta R/R$, was measured at a near-normal incidence from the cleaved surfaces.

The pump and probe beam diameters were 40-70 and 18-30 μm , respectively. The probe fluence was $\sim 5 \mu\text{J}/\text{cm}^2$ for all measurements. The Polarizations of pump and probe beams were perpendicular to each other with a random orientation with respect to the crystal axes. The transient reflectivity showed no polarization dependence.

B. Results

In Fig. 2 (a) we show the transient reflectivity in sample S1¹⁸ at a few characteristic T measured at weak excitation¹⁹ of $F = 150 \mu\text{J}/\text{cm}^2$ on a warming run. In the low- T insulating phase we observe a clear weakly damped coherent-phonon response that is only slightly T -dependent. The beating pattern indicates the presence of several modes. Fourier transform spectra [Fig. 2 b)] reveal two stronger modes at 1.85 and 2.34 THz together with three weaker modes at 3.24, 3.32 and 3.76 THz. All the modes soften and broaden with increasing T and suddenly disappear at $T_{\text{IM}\uparrow} = 235 \text{ K}$ while on cooling they suddenly appear at $T_{\text{IM}\downarrow} = 233 \text{ K}$. In the metallic phase above $T_{\text{IM}}^{\text{20}}$ we observe no coherent modes and no relaxation²¹ on the 30-ps time scale of the experiment.

III. ANALYSIS

A. Data fitting

The transient reflectivity data were analysed in the framework of the displacive excitation of coherent phonons (DECP) theory²³ (Appendix). The experimental transient reflectivity in the low- T insulating phase can be fairly described assuming an exponentially relaxing electronic displacive component with the relaxation time $\tau_{\text{displ}}^{\text{24}}$ in the picosecond range that drives five oscillatory lattice modes with the frequencies, Ω_i , dampings, γ_i , and amplitudes, $A_{\text{O}i}$. An additional exponential component needs to be included to completely describe the relaxation at low T (see Fig. 3).

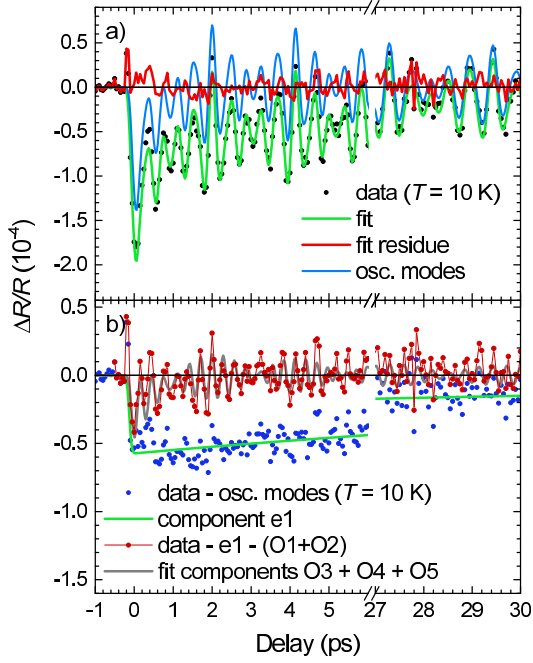


Figure 3. Illustration of different DECP model components in sample S1 at $T = 10$ K. a) The total oscillatory part of the fit in comparison to the data, fit and fit residue. b) Subtraction of various model component combinations from the data with the corresponding remaining fit components.

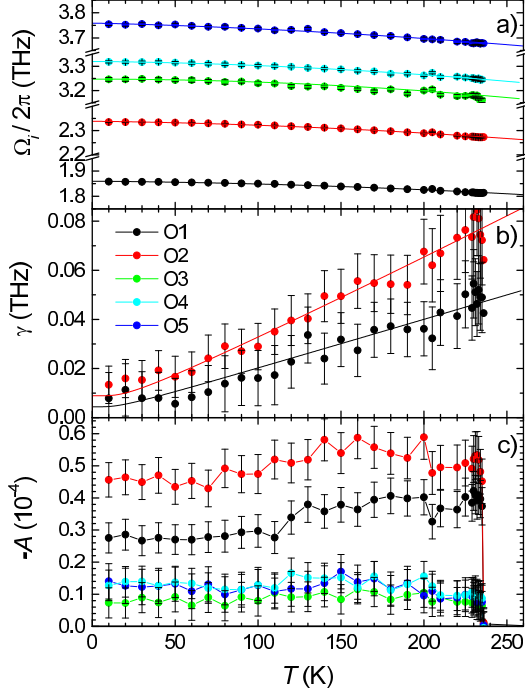


Figure 4. Temperature dependence of the coherent phonon parameters from DECP fits on warming. The thin lines in a) are the anharmonic theory fits of Eq. (3.9) from²² and in b) fits of Eq. (3.8) from²².

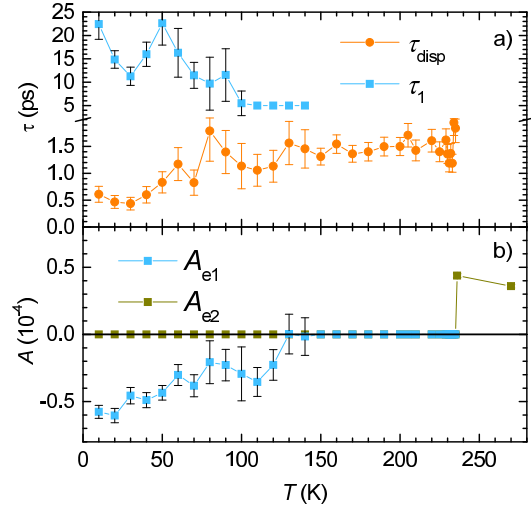


Figure 5. Temperature dependence of the exponential fit-components parameters at low excitation fluence from DECP fits on warming.

Due to the small amplitudes of the three weakest coherent modes (O3, O4, O5) the corresponding dampings showed large scattering and caused fit instability. In order to prevent the adverse influence to the fit convergence we fixed the three weakest modes γ_i to 0.03 THz. The fixed values of the dampings were chosen to approximately correspond to the values determined for the strongest modes O1 and O2 in the middle of the relevant T range. Since the scan lengths are comparable or shorter than γ_i^{-1} this introduces only some systematic bias to the amplitudes of these modes, but does not affect significantly their frequencies and the other-components fit parameters.

It turns out that we can fit the data setting the dispersive component amplitude, $A_{\text{displ}} = 0$, in the full T -range below T_{IM} indicating that the dispersive component only weakly couples to the transient reflectivity at $\hbar\omega = 1.55$ -eV. Below ~ 130 K, however, inclusion of an additional exponentially relaxing component with $\tau_1 \sim 15$ ps and amplitude A_{e1} was necessary to completely fit the transient response.

In Figs. 4 and 5 we show the temperature dependence of the DECP theory parameters. The coherent modes amplitudes show no or a rather weak T dependence in the low- T insulating phase dropping abruptly to zero above T_{IM} . With increasing T the modes show softening of about $\sim 2\%$ accompanied by a more significant damping increase. Both, the softening and the damping increase can be attributed to the lattice anharmonicity.²²

Above T_{IM} the data can be fit by a double exponential response with the relaxation times $\tau \sim 100$ fs and $\tau_{e2} \gg 30$ ps.²⁵ Below T_{IM} both components abruptly vanish.

Raman ^a ($T = 83$ K) (cm^{-1})	$\Delta R/R^b$ ($T = 150$ K) (cm^{-1})	$\Delta R/R^c$ ($T = 10$ K) (cm^{-1}) (THz)
γ^d	-	62 1.86
γ^d	-	78 2.34
γ^d	85	- -
109	-	108 3.25
120 ^e	-	111 3.32
-	139	125 3.76
145	-	- -
172	-	173 5.2 ^f
203	-	200 5.69 ^f

^a Zhang *et al.*, Ref. [7]

^b Matsubara *et al.*, Ref. [9]

^c present work

^d Out of the measurement range in Ref. [7].

^e In the metallic state at room T (our data).

^f Barely observable by averaging several low- T spectra.

Table I. Comparison of the observed low- T Raman-/coherent-mode frequencies in different experiments.

B. Discussion

The high- T space group of CuIr_2S_4 is $Fd\bar{3}m$ leading to five distinct Raman lines corresponding to the $1A_g + 1E_g + 3F_{2g}$ irreducible representations.⁷ The Raman tensor of the A_g mode is diagonal and isotropic²⁶ so the scattering in the back scattering geometry is allowed for parallel excitation-scattering polarizations and suppressed for the perpendicular polarizations for any light propagating direction.

The nonzero Raman tensor components for the degenerate E_g representations are (i) $\chi_{xx}^{E_g}(1) = \chi_{yy}^{E_g}(1) = b$, $\chi_{zz}^{E_g}(1) = -2b$ and (ii) $\chi_{xx}^{E_g}(2) = -\chi_{yy}^{E_g}(2) = -\sqrt{3}b$. The scattering²⁷ is suppressed only for the crossed polarizations parallel to the $\langle 100 \rangle$ directions.

The nonzero Raman tensor components for the triply-degenerate F_{2g} representations are: $\chi_{ij}^{F_{2g}}(k) = \chi_{ji}^{F_{2g}}(k)$ where $ij \equiv xy, xz$ and yz for $k = 1, 2$ and 3 , respectively. The scattering is suppressed only for the crossed polarizations parallel to the $\langle 110 \rangle$ directions.

In sample S1 only the A_g mode is suppressed in the crossed polarization due to the low symmetry surface orientation. On the other hand, in sample S2 systematic extinctions consistent with the back-scattering along the $[001]$ direction were observed for different polarization configurations implying that the orientation of the S2 cleaved surface corresponds to a $\langle 001 \rangle$ plane.

The observed polarization dependence of the additional weak line at 120 cm^{-1} is consistent with the F_{2g} representation in both samples and is therefore attributed to the previously unobserved⁷ $F_{2g}(3)$ modes.

The coherent-mode frequencies and the number of the observed coherent modes are different than reported previously⁹ (see Table I). Sample S2 has identical orientation²⁸ of the measured surface as reported in Ref.

[9] and the excitation and probe photon energies are also the same. Moreover, the modes reported in Ref. [9] are insensitive to the IM transition. It is therefore very likely that the transient response reported in Ref. [9] is not intrinsic.

A better correspondence is found to the low- T Raman mode frequencies⁷. In the overlap region²⁹ we observe a correspondence of the coherent mode doublet at $108/111 \text{ cm}^{-1}$ to the broad Raman line at 109 cm^{-1} . We also observe weak signs of modes³⁰ (not shown in Fig. 2) at the 172-cm^{-1} and 203-cm^{-1} Raman mode positions.

On the other hand, the coherent mode at 125 cm^{-1} is absent in the low- T Raman spectra⁷ and the low- T Raman mode⁷ at 145 cm^{-1} is absent in the coherent response. However, the 120-cm^{-1} room- T frequency of the newly observed weak $F_{2g}(3)$ mode is close to the 125-cm^{-1} coherent mode frequency so the mode could be linked to the $F_{2g}(3)$ mode that hardens³¹ and changes the symmetry to A_g upon entering the low- T insulating state. In the high- T state it is absent from the coherent response since it cannot be excited by the dispersive mechanism due to the F_{2g} symmetry. According to the low- T symmetry the mode should also split to three A_g modes³², but this is not observed in the experiment.

Since there is no selection-rules-forbidden³³ modes at low- T in both experiments we attribute the absence of the 145-cm^{-1} mode in the coherent response to different Raman resonance conditions.

The low- T lattice-structure⁴ primitive cell is large and has low symmetry (PI) so 84 A_g modes are Raman allowed.²⁶ Looking at the low frequency range the heaviest Ir ions contribute 24 and Cu ions further 12 A_g modes to the mechanical representation while in the high- T phase Ir ions do not contribute to the Raman allowed modes at all.

In experiments only 8 modes are observed below $\sim 200 \text{ cm}^{-1}$. This is consistent with proximity^{4,6} of the structure to the $I4_1/amd$ (D_{4h}) symmetry where the Ir ions are not Raman active and the Cu ions contribute to the one B_{1g} and one E_g symmetry mode only, which corresponds to the 120-cm^{-1} $F_{2g}(3)$ mode of the high- T phase.

Among the 8 observed modes the 125-cm^{-1} (3.76-THz) related $F_{2g}(3)$ mode does not contain Ir-ions displacements in the high- T phase so it is expected to remain Cu-ions displacements dominated in the low- T phase as well. The two lowest frequency modes at 62 cm^{-1} (1.86 THz) and 78 cm^{-1} (2.34 THz) are therefore expected to be the most closely related to the vibrations of the dimerized Ir^{+4} ions that shift the most at the IM phase transitions.

Turning to the non-oscillating relaxation dynamics it is unexpected that there is no clear relaxation component due to the recombination of the photoexcited quasiparticle across the gap in the low- T state. The observed 15-ps exponential relaxation is not correlated with the gap opening since it clearly appears only well below the T_{IM} .³⁴ The experimentally reported gap³⁵ of 150 meV (1200 cm^{-1}) significantly exceeds the maximum phonon

frequency of $\sim 500 \text{ cm}^{-1}$. A relaxation slower than our experimental time window is therefore expected due to the recombination since single phonon processes are forbidden. The absence of such component therefore suggests that the optical transitions at 1.55-eV do not involve states at the gap edges.

IV. SUMMARY AND CONCLUSIONS

We performed a room- T Raman and systematic T -dependent investigation of the ultrafast transient reflectivity in CuIr_2S_4 .

In the Raman spectra we observe an additional previously undetected F_{2g} mode at 120 cm^{-1} .

The transient reflectivity in the low- T insulating phase at 1.55-eV photon energy is dominated by the broken-lattice-symmetry-induced coherent lattice response that abruptly vanishes at the insulator-metal transition. The frequencies of the coherent modes are different from previously reported transient reflectivity study⁹, but consistent with the published low- T Raman spectra⁷. The coherent modes show a rather standard anharmonic T -dependence in the full insulating phase T -range.

ACKNOWLEDGMENTS

The authors acknowledge the financial support of Slovenian Research Agency (research core funding No-

P1-0040 and) for financial support. We would also like to thank V. Nasretidnova and E. Goreschnik for the help at the sample characterization.

V. APPENDIX

A. DECP model fits

To analyze the signal we fit the data using the DECP model²³ where the transient reflectivity is given by

$$\begin{aligned} \frac{\Delta R}{R} = & (A_{\text{displ}} + \sum A_{O_i}) \int_0^\infty G(t-u) e^{-u/\tau_{\text{displ}}} du \\ & - \sum A_{O_i} \int_0^\infty G(t-u) e^{-\gamma_i u} [\cos(\Omega_i u) \\ & \quad - \beta_i \sin(\Omega_i u)] du \\ & + \sum A_{e_j} \int_0^\infty G(t-u) e^{-u/\tau_j} du, \end{aligned} \quad (1)$$

where $\beta_i = (1/\tau_{\text{displ}} - \gamma_i)/\Omega_i$ and $G(t) = \sqrt{2/\pi}\tau_p \exp(-2t^2/\tau_p^2)$ with τ_p being the effective pump-probe pulse cross-correlation width. In the DECP model the coherent modes are driven with an exponentially relaxing dispersive mode with the relaxation time τ_{displ} and the amplitude, A_{displ} ³⁶. A_{O_i} , Ω_i , γ_i are the oscillating modes amplitudes, frequencies and damping factors, respectively, while A_{e_j} and τ_j are the amplitudes and relaxation times of additional exponentially relaxing modes.

* tomaz.mertelj@ijs.si

¹ S. Nagata, T. Hagino, Y. Seki, and T. Bitoh, *Physica B: Condensed Matter* **194**, 1077 (1994).
² M. Isobe and Y. Ueda, *Journal of the Physical Society of Japan* **71**, 1848 (2002), <https://doi.org/10.1143/JPSJ.71.1848>.
³ D. Khomskii and T. Mizokawa, *Physical review letters* **94**, 156402 (2005).
⁴ P. G. Radaelli, Y. Horibe, M. J. Gutmann, H. Ishibashi, C. Chen, R. M. Ibberson, Y. Koyama, Y.-S. Hor, V. Kiryukhin, and S.-W. Cheong, *Nature* **416**, 155 (2002).
⁵ M. Schmidt, I. W Ratcliff, P. Radaelli, K. Refson, N. Harrison, and S.-W. Cheong, *Physical review letters* **92**, 056402 (2004).
⁶ T. Furubayashi, T. Matsumoto, T. Hagino, and S. Nagata, *Journal of the Physical Society of Japan* **63**, 3333 (1994).
⁷ L. Zhang, L. Ling, Z. Qu, W. Tong, S. Tan, and Y. Zhang, *The European Physical Journal B* **77**, 83 (2010).
⁸ L. Zhang, L. Ling, J. Fan, R. Zhang, C. Xi, X. Zhu, C. Zhang, and Y. Zhang, *Journal of magnetism and magnetic materials* **330**, 12 (2013).
⁹ I. Matsubara, S. Ebihara, T. Mishina, J. Nakahara, N. Matsumoto, and S. Nagata, *Phys. Rev. B* **79**, 054110 (2009).
¹⁰ H. Ishibashi, T. Koo, Y. S. Hor, A. Borisso, P. G. Radaelli, Y. Horibe, S. Cheong, and V. Kiryukhin, *Physical Review*

B **66**, 144424 (2002).

¹¹ T. Furubayashi, H. Suzuki, T. Matsumoto, and S. Nagata, *Solid state communications* **126**, 617 (2003).
¹² K. Takubo, S. Hirata, J.-Y. Son, J. Quilty, T. Mizokawa, N. Matsumoto, and S. Nagata, *Physical review letters* **95**, 246401 (2005).
¹³ V. Kiryukhin, Y. Horibe, Y. S. Hor, H. Noh, S. Cheong, and C. Chen, *Physical review letters* **97**, 225503 (2006).
¹⁴ K. Takubo, T. Mizokawa, N. Matsumoto, and S. Nagata, *Physical Review B* **78**, 245117 (2008).
¹⁵ E. Božin, A. S. Masadeh, Y. S. Hor, J. Mitchell, and S. Billinge, *Physical review letters* **106**, 045501 (2011).
¹⁶ N. Matsumoto and S. Nagata, *Journal of crystal growth* **210**, 772 (2000).
¹⁷ L. Stojchevska, M. Borovšak, P. Foury-Leylekian, J.-P. Pouget, T. Mertelj, and D. Mihailovic, *Phys. Rev. B* **96**, 035429 (2017).
¹⁸ Both samples show identical T -dependence.
¹⁹ The linearity of the response at this fluence was checked at 6 K, 190 K, 245 K and 270 K.
²⁰ Due to the presence of small hysteresis we use $T_{\text{IM}\uparrow}$ or $T_{\text{IM}\downarrow}$ when we refer to the warming or cooling runs, respectively, and T_{IM} when we do not care about the the temperature change direction.
²¹ The traces show a hint of a weak sub-ps relaxation component that is obscured by the coherent artifact.

- ²² M. Balkanski, R. F. Wallis, and E. Haro, Phys. Rev. B **28**, 1928 (1983).
- ²³ H. Zeiger, J. Vidal, T. Cheng, E. Ippen, G. Dresselhaus, and M. Dresselhaus, Physical Review B **45**, 768 (1992).
- ²⁴ Please see Appendix for the detailed definition.
- ²⁵ The long lived component shows no relaxation in the experimental time window.
- ²⁶ E. Kroumova, M. Aroyo, J. Perez-Mato, A. Kirov, C. Capillas, S. Ivantchev, and H. Wondratschek, Phase Transitions **76**, 155 (2003), <https://doi.org/10.1080/0141159031000076110>.
- ²⁷ Simultaneously for both degenerate modes.
- ²⁸ Due to the low point symmetry of the low- T insulating phase it is also very unlikely that the difference could be due to the different orientations of the measured surfaces and the correspondingly different selection rules.
- ²⁹ The published⁷ Raman spectra start at 100 cm^{-1} and the present experiment time resolution limits the maximum coherent-mode frequency below the cutoff of $\sim 300\text{ cm}^{-1}$.
- ³⁰ The modes are so weak that a reliable identification is possible only by averaging all transients measured below T_{IM} .
- ³¹ The coherent mode frequency just below T_{IM} is 122.7 cm^{-1} .
- ³² For the approximate⁴ $I4_1/amd$ (D_{4h}) group the splitting would be twofold into $B_{1g} + E_g$ modes.
- ³³ Due to the low point-group symmetry (C_i) of the low- T phase all Raman active modes correspond to the A_g representation.
- ³⁴ From the present data it is not clear whether the 15-ps exponential relaxation is the photoexcited quasiparticle related since it can also correspond to the incoherent-phonons induced band renormalizations.
- ³⁵ N. Wang, G. Cao, P. Zheng, G. Li, Z. Fang, T. Xiang, H. Kitazawa, and T. Matsumoto, Physical Review B **69**, 153104 (2004).
- ³⁶ A_{displ} represents the coupling of the displacive mode to the optical reflectivity while the couplings to different oscillatory modes are implicitly included in parameters A_{O_i} .